A Meshfree Numerical Method for Acoustic Wave Propagation Problems in Planar Domains with Corners and Cracks

Pedro R. S. Antunes[a], Svilen S. Valtchev[*,b]

[a] *Group of Mathematical Physics of the University of Lisbon, Complexo Interdisciplinar, Av. Prof. Gama Pinto 2, P-1649-003 Lisbon, Portugal*
[b] *CEMAT, Instituto Superior Técnico, TU Lisbon, Av. Rovisco Pais, 1049-001 Lisbon, Portugal and Department of Mathematics, ESTG, Instituto Politécnico de Leiria, Leiria, Portugal*

Abstract

The numerical solution of acoustic wave propagation problems in planar domains with corners and cracks is considered. Since the exact solution of such problems is singular in the neighborhood of the geometric singularities the standard meshfree methods, based on global interpolation by analytic functions, show low accuracy. In order to circumvent this issue, a meshfree modification of the Method of Fundamental Solutions is developed, where the approximation basis is enriched by an extra span of corner adapted non-smooth shape functions. The high accuracy of the new method is illustrated by solving several Boundary Value Problems for the Helmholtz equation, modelling physical phenomena from the fields of room acoustics and acoustic resonance.

Key words: Meshfree methods, Method of Fundamental Solutions, Singular problems, Acoustic wave propagation, Room acoustics, Acoustic resonance
2000 MSC: : 35J05, 35E05, 65N25, 65N35, 74J20, 65Y99

1. Introduction

In this work we address the numerical solution of Boundary Value Problems (BVP) for the Helmholtz equation, also known as the *reduced wave equation*. Such problems arise when modelling the propagation of time-harmonic acoustic waves with low amplitudes in homogeneous media. From an application's point of view, we will be interested in the approximate solution of interior scattering problems and acoustic resonance problems in planar domains with non-smooth geometries.

Let $\Omega \subset \mathbb{R}^2$ be a bounded domain with boundary $\Gamma = \Gamma_1 \cup \Gamma_2$ and consider the following BVP for the Helmholtz homogeneous Partial Differential Equation (PDE)

$$\begin{cases} \Delta u + k^2 u = 0 & \text{in } \Omega \\ u = g_1 & \text{on } \Gamma_1 \\ \partial_\nu u = g_2 & \text{on } \Gamma_2, \end{cases} \tag{1}$$

where, for a unitary speed of wave propagation, $k > 0$ denotes the wave-frequency, g_1 and g_2 are prescribed Dirichlet and Neumann boundary conditions (BC), ν is the normal vector at Γ_2, pointing outwards with respect to Ω and $\partial_\nu u$ is the normal derivative of the unknown solution u at Γ_2. BVP (1) is well posed, except for a countable number of eigenfrequencies k, for which the homogeneous problem (with $g_1 = g_2 = 0$) has non-trivial solutions, e.g. [15, 11].

*Corresponding author
Email addresses: pant@math.ist.utl.pt (Pedro R. S. Antunes), ssv@math.ist.utl.pt (Svilen S. Valtchev)

From a numerical point of view, the methods developed here will be based on the classical Method of Fundamental Solutions (MFS), e.g. [30], which is a meshfree technique used for the approximate solution of Boundary Value Problems for homogeneous PDEs. In particular, the MFS is a boundary collocation method, where the unknown solution is approximated by superposition of fundamental solutions of the corresponding differential operator, e.g. [37]. It has been applied successfully for the solution of a variety of physical problems in fluid mechanics, acoustics, electromagnetism, elasticity and options pricing. The reported numerical results indicate that highly accurate approximate solutions may be obtained at a relatively low computational cost, provided the boundary of the domain Ω and the boundary conditions of the BVP are sufficiently regular. A list of applications of the MFS and related variants may be found in the survey papers [19, 20, 22] and in the book [23].

On the other hand, the standard MFS may experience significant difficulties when applied to BVPs in domains with corners or cracks. This problem is due to the fact that the solution u or some of its derivatives are singular at the referred corners' (cracks') tips. Consequently, no linear combination of the analytic shape functions will provide a high precision local approximation. From this point of view, a modification of the MFS's formulation is required in order to extend its range of application to such singular problems. Here, we will develop an enrichment technique, where the MFS basis is augmented by a set of singular, corner (crack) adapted, particular solutions of the Helmholtz PDE. Similar approach was considered in [4] for a crack analysis problem involving the Dirichlet BVP for the Laplace equation.

In section 2 we include a brief review of the numerical formulation of the classical MFS, as well as some theoretical and numerical considerations related to its application. A set of corner adapted particular solutions of the Helmholtz PDE is derived in section 3, for the Dirichlet, Neumann and mixed Dirichlet-Neumann BVPs. The enriched MFS is formulated in section 4, for the non-resonance and the resonance problems. Numerical simulations, illustrating the high accuracy of the new method, will be presented in section 5.

2. The Method of Fundamental Solutions

A fundamental solution of the 2D Helmholtz differential operator is given by the radially symmetric spherical wave

$$\Phi_k(x) = \frac{i}{4} H_0^{(1)}(k|x|), \quad x \in \mathbb{R}^2 \backslash \{0\},$$

which satisfies (in the distributional sense) the equation $(\Delta + k^2)\Phi_k = -\delta$. Here, δ is the Dirac delta distribution, centered at $x = 0$ and $H_0^{(1)} = J_0 + iY_0$ is the Hänkel function, defined through the Bessel functions of the first and second kind J_0 and Y_0, respectively. As a consequence of the singularity of the Bessel function Y_0 the fundamental solution is also singular at its center of symmetry $x = 0$. By shifting this singularity to an exterior point $y \notin \bar{\Omega}$, referred to as the *source point* of Φ_k, we obtain a particular solution $\Phi_k(\cdot - y)$ of the Helmholtz equation in $\bar{\Omega}$.

In the classical MFS the unknown solution of the BVP (1) is approximated by a linear combination of fundamental solutions

$$u(x) \approx u_n(x) = \sum_{j=1}^{n} \alpha_j \Phi_k(x - y_j), \quad x \in \bar{\Omega}, \tag{2}$$

with unknown coefficients $\boldsymbol{\alpha} = (\alpha_1, \ldots, \alpha_n) \in \mathbb{C}^n$ and source points (singularities)

$$\mathcal{Y} = \{y_j \in \hat{\Gamma} : \ j = 1, \ldots, n\},$$

selected on an admissible *pseudo boundary* $\hat{\Gamma}$, e.g. [2], embracing Ω, see Fig. 1. Note that, by its definition, u_n is readily a particular solution of the Helmholtz equation in $\bar{\Omega}$.

In order to calculate $\boldsymbol{\alpha}$ we have to enforce that u_n satisfies the boundary conditions from (1) with respect to a set of boundary collocation points $\mathcal{X} \subset \Gamma$. More precisely, we consider the two point sets

$$\mathcal{X}_1 = \{x_i \in \Gamma_1 : \ i = 1, \ldots, m_1\}$$

$$\mathcal{X}_2 = \{x_i \in \Gamma_2 : \ i = m_1 + 1, \ldots, m_1 + m_2\}$$

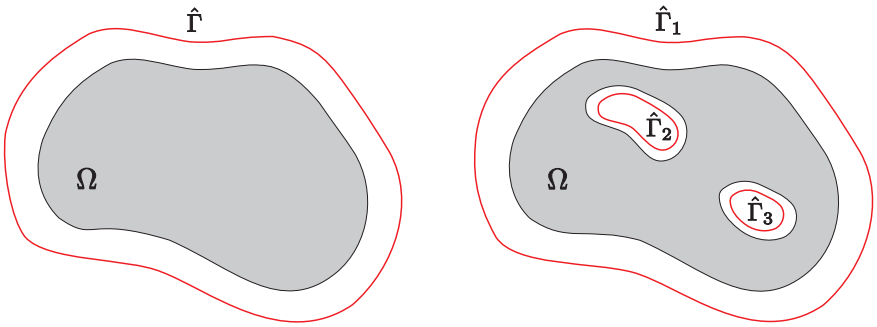

Figure 1: A simply connected domain Ω and pseudo-boundary $\hat{\Gamma}$ (left) and a multiply connected domain with two holes and pseudo-boundary $\hat{\Gamma} = \hat{\Gamma}_1 \cup \hat{\Gamma}_2 \cup \hat{\Gamma}_3$ (right).

and impose the boundary conditions as follows

$$\begin{cases} u_n(x_i) = g_1(x_i), \quad x_i \in \mathcal{X}_1 & (\textit{Dirichlet BC}) \\ \partial_\nu u_n(x_i) = g_2(x_i), \quad x_i \in \mathcal{X}_2 & (\textit{Neumann BC}) \end{cases}$$

Let $\mathcal{X} := \mathcal{X}_1 \cup \mathcal{X}_2$ with $\mathcal{X}_1 \cap \mathcal{X}_2 = \emptyset$ and define $m := m_1 + m_2$ for the total number of boundary collocation points.

In the case of BVP (1), i.e. when two types of boundary conditions are imposed on subsets of Γ, the MFS approximation leads to the solution of a $m \times n$ linear system of the form

$$\begin{bmatrix} \mathbf{A}_1 \\ - - - - - \\ \mathbf{A}_2 \end{bmatrix} \begin{bmatrix} \alpha_1 \\ \vdots \\ \alpha_n \end{bmatrix} = \begin{bmatrix} \boldsymbol{g}_1 \\ -- \\ \boldsymbol{g}_2 \end{bmatrix}. \tag{3}$$

Here the blocks corresponding to the boundary conditions are given by

$$\mathbf{A}_1 = [\Phi_k(x_i - y_j)]_{m_1 \times n} \quad \text{and} \quad \boldsymbol{g}_1 = [g_1(x_i)]_{m_1 \times 1}, \tag{4}$$

for the Dirichlet BC and

$$\mathbf{A}_2 = [\partial_\nu \Phi_k(x_i - y_j)]_{m_2 \times n} \quad \text{and} \quad \boldsymbol{g}_2 = [g_2(x_i)]_{m_2 \times 1}, \tag{5}$$

for the Neumann BC. Define the total collocation matrix by $\mathbf{A} := [\mathbf{A}_1 \;\; \mathbf{A}_2]$ and the right-hand-side vector by $\boldsymbol{g} := [\boldsymbol{g}_1 \;\; \boldsymbol{g}_2]$.

The two most popular methods for solving system (3) are by collocation, when $n = m$, and by a least squares approach, when the system is over-determined, i.e. when $m > n$. In the second case we solve the corresponding square system of normal equations

$$\mathbf{A}^* \mathbf{A} \boldsymbol{\alpha} = \mathbf{A}^* \boldsymbol{g},$$

where $\mathbf{A}^*$ denotes the conjugate transpose of the matrix $\mathbf{A}$. Explicitly, the solution of the square linear systems may be calculated by Gauss elimination, whenever the matrix $\mathbf{A}$ is well conditioned. However, in most simulations $\mathbf{A}$ is ill-conditioned or even singular within the machine precision, e.g. [10, 33], and a pseudo inversion technique, e.g. Tikhonov regularization or Truncated Singular Value Decomposition (TSVD), is required for the solution of (3). The ill-conditioning of $\mathbf{A}$ is related to the theoretical origin of the MFS. More precisely, the MFS may be seen as a discretization of a Fredholm integral equation of the first kind with a compact kernel. Consequently, the ill-posedness of the continuous model carries over to the discrete problem in the form of ill-conditioning.

Note that, due to the analyticity of the shifted fundamental solutions in Ω, the approximate solution u_n is also analytic in Ω. Therefore, approximations of the derivatives of the solution at any point $x \in \Omega$ may be easily calculated by a term-wise differentiation in (2). The latter is a non-trivial task when standard element-based methods, such as the Finite Element Method and the Boundary Element Method, are applied.

The MFS, as described above, shows high accuracy when applied to BVPs in smooth settings. The numerical results may be improved considerably by increasing the number of source and collocation points or by increasing the distance between the boundary and the pseudo boundary, e.g. [10, 7, 29]. The situation changes dramatically when domains with boundary singularities, e.g. corners, are considered. In this case, the analytic shape functions $\Phi_k(\cdot - y_j)$ fail to approximate the correct, singular local behavior of the exact solution at the corner's tip.

One solution for the corner problem is to free some of the source points and to use the nonlinear version of the MFS, see Remark 1, of course, with a very restricted number of nonlinear parameters. Usually five or six free source points will treat the problem for any singularity, see [18]. Another possibility is to enrich the nonlinear MFS with additional functions, which describe the correct local behavior of the solution at the corner, e.g. [26, 36]. However, both these variants require the solution of a nonlinear minimization problem for the unknown coefficients α_j, sources' locations y_j and, possibly, for some unknown parameters of the extra shape functions. In the following section we will introduce an enrichment technique, based on the standard MFS (with fixed source points), which preserves the simplicity and the linearity of the original method.

Remark 1. Instead of taking a pre-fixed set of singularities $\mathcal{Y}$ one could also consider a nonlinear variant of the MFS, where the locations y_j of the source points have to be determined along with the coefficients α_j. In this case we have to solve a nonlinear minimization problem. Since non-uniqueness of solution may occur and also, from a computational point of view, this modification of the MFS is significantly more expensive it will not be considered in this work. For further details on this approach see [34, 18].

3. Corner adapted shape functions

Consider the homogeneous Helmholtz equation, represented in polar coordinates (r, θ)

$$\left(\partial_r^2 + \frac{1}{r}\partial_r + \frac{1}{r^2}\partial_\theta^2 + k^2\right) u(r,\theta) = 0, \quad (r,\theta) \in [0,\infty[\times[0,2\pi[. \tag{6}$$

Through separation of variables we can calculate the following family of particular solutions of (6)

$$u(r,\theta) = \left[c_1 J_\mu(kr) + c_2 Y_\mu(kr)\right] \times \left[c_3 \sin(\mu\theta) + c_4 \cos(\mu\theta)\right],$$

where $c_i \in \mathbb{C},\ i = 1, \ldots, 4$ and $\mu > 0$ are arbitrary constants and J_μ and Y_μ are Bessel functions of first and second kind and order μ. Avoiding the Bessel Y_μ functions, which are singular at the pole $r = 0$, we define the two sets of continuous particular solutions of (6)

$$\phi(r,\theta) := J_\mu(kr)\sin(\mu\theta) \quad \text{and} \quad \psi(r,\theta) := J_\mu(kr)\cos(\mu\theta), \qquad \mu > 0. \tag{7}$$

Let $\Omega \subset \mathbb{R}^2$ be a polar sector (unbounded wedge) with interior angle $\pi/\omega,\ \omega \geq 1/2$, see Fig. 2-left. From (7) we will derive particular solutions to the Helmholtz equation coupled with homogeneous (null) Dirichlet, Neumann and mixed Dirichlet-Neumann boundary conditions on $\overrightarrow{OA}$ and $\overrightarrow{OB}$. Such solutions will be used as extra shape functions for the enriched MFS, developed in section 4.

Dirichlet boundary conditions. From the expression of $\phi(r,\theta)$ we calculate $\mu > 0$ such that $\phi(r,\theta) = 0$ for $\theta = 0$ and $\theta = \pi/\omega$. Explicitly, we obtain $\mu = s\omega$, with $s \in \mathbb{N}$, and define the family of particular solutions

$$\phi_s(r,\theta) = J_{s\omega}(kr)\sin(s\omega\theta), \quad s \in \mathbb{N}. \tag{8}$$

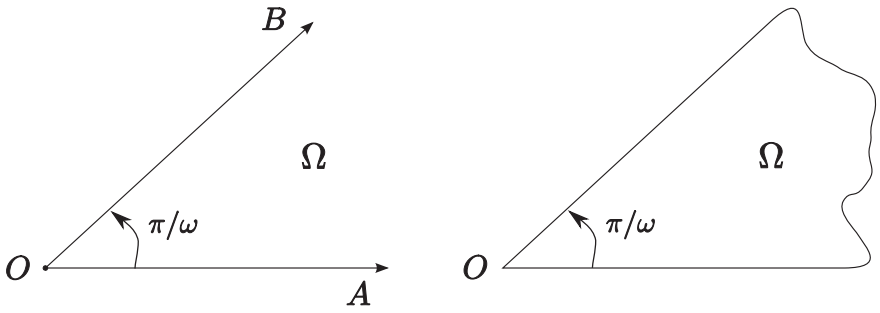

Figure 2: A wedge domain with an interior angle π/ω (left) and a domain with one corner (right).

Graphical examples of the functions $\phi_s \in C^\infty(\Omega) \cap C(\bar{\Omega})$ are shown in Fig. 3. According to their definition, ϕ_s are eigenfunctions for the Dirichlet BVP in the unbounded wedge domain Ω. These functions have been frequently used for the numerical solution of Dirichlet eigenproblems for the Laplace operator, e.g. [21, 9]. When exclusively ϕ_s are employed as shape functions the corresponding discrete boundary collocation method is known as the Method of Particular Solutions (MPS).

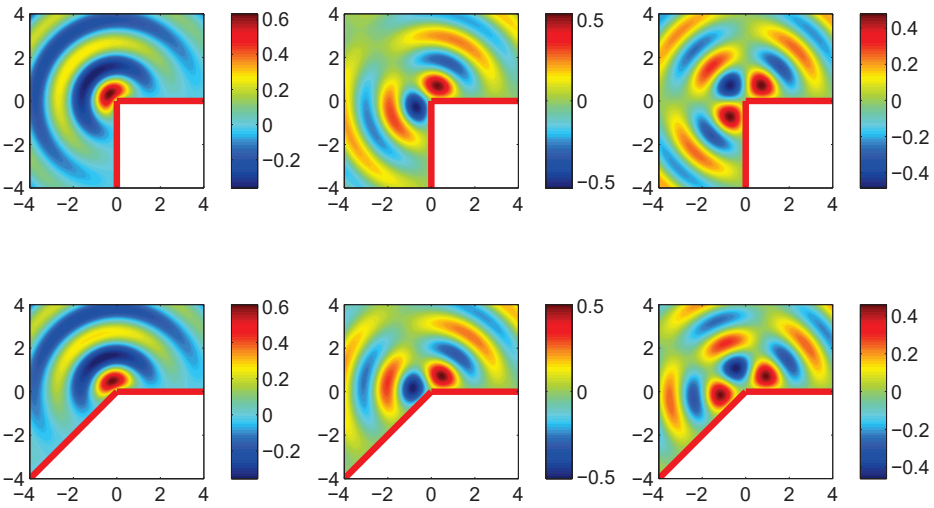

Figure 3: The local behavior of the functions ϕ_s for $k = 3$, $s = 1, 2, 3$, $\omega = 2/3$ (first row) and $\omega = 4/5$ (second row).

Neumann boundary conditions. From Fig. 2-left we note that the normal derivative at the boundary of the wedge domain is $\partial_\nu \equiv -\partial/\partial\theta$ on $\overrightarrow{OA}$ and $\partial_\nu \equiv \partial/\partial\theta$ on $\overrightarrow{OB}$. Direct calculation shows that the normal derivative of the functions

$$\psi_s(r, \theta) = J_{s\omega}(kr)\cos(s\omega\theta), \quad s \in \mathbb{N} \tag{9}$$

on Γ is $\partial_\nu \psi_s(r, \theta) = \pm s\omega\phi_s(r, \theta)$ and we have $\partial_\nu \psi_s(r, \theta) = 0$ for $\theta = 0$ and $\theta = \pi/\omega$. Consequently, ψ_s are Neumann eigenfunctions for the Laplace operator in the wedge domain, e.g. [17]. Again, $\psi_s \in C^\infty(\Omega) \cap C(\bar{\Omega})$.

Mixed Dirichlet-Neumann boundary conditions. When BVPs with mixed Dirichlet-Neumann boundary conditions are considered, eventually, we may have a Dirichlet condition on one edge of a corner and a Neumann condition on the other. This situation may be treated by a combination of the previous two approaches. In

particular, the $C^\infty(\Omega) \cap C(\bar{\Omega})$ functions

$$\varphi_s(r,\theta) = \phi_{s-1/2}(r,\theta) = J_{(s-1/2)\omega}(kr)\sin((s-1/2)\omega\theta), \quad s \in \mathbb{N} \tag{10}$$

satisfy $\varphi_s(r,\theta) = 0$ on $\overrightarrow{OA}$ and $\partial_\nu \varphi_s(r,\theta) = 0$ on $\overrightarrow{OB}$, for the wedge domain.

Note that, if we exchange the boundary conditions, i.e. for a Neumann BC on $\overrightarrow{OA}$ and a Dirichlet BC on $\overrightarrow{OB}$, the appropriate shape functions are $\varphi_s := \psi_{s-1/2},\ s \in \mathbb{N}$.

Remark 2. Corners with $\omega \in \mathbb{N}$ are called *regular* and, usually, they represent no difficulties for the classical MFS, formulated in section 2. On the other hand, for $\omega \notin \mathbb{N}$ the corners are referred to as *singular* and the MFS shows numerical results with unsatisfactory accuracy. Enrichment of the approximation basis is required here. The difference between the two types of corners is related to the existence of an analytic extension (by reflection) of ϕ_s and ψ_s to the whole plane, e.g. [16, 9]. For singular corners such extension is not possible and ϕ_s and ψ_s have a branch point at the corner's tip. In general, the proposed corner adapted shape functions will exhibit singular behavior whenever Bessel functions of non integer orders are involved, also see (20).

4. The enriched Method of Fundamental Solutions

As we mentioned before, the standard MFS does not show satisfactory accuracy when applied for the solutions of boundary value problems in singular geometries, such as regions with reentrant corners or cracks. The problem here is that the exact solution u of the BVP is singular at the corner's (crack's) tip. For example, Lehmann [31] showed that for an eigenfunction u of a region with an interior angle of magnitude π/ω, $\omega \in \mathbb{R}\backslash\mathbb{Q}$ there exists a constant γ such that in a neighborhood of the corner

$$u(r,\theta) = \gamma\ r^\omega \sin(\omega\theta) + o\left(r^\omega\right),$$

i.e. some of the derivatives of the eigenfunction are singular at the corner's tip. Similar behavior is exhibited by the BVP's solution u in the non resonance case, e.g. [25].

In order to develop an accurate numerical method it is important that the shape functions can reproduce correctly the singular behavior of the exact solution. We will assume that the solution of the BVP (1) can be decomposed as a sum of a regular and a singular parts,

$$u(x) = u_R(x) + u_S(x), \quad x \in \Omega. \tag{11}$$

A classical MFS expansion (2) will be used for the approximation of u_R, i.e. for the regular part of the solution. The main idea of the MFS variant developed here is to augment the original approximation basis by an extra span of singular particular solutions of Helmholtz PDE that can approximate accurately u_S, i.e. the singular part of the solution.

4.1. The non-resonance case

In the non-resonance case, we assume that k is not an eigenfrequency for the BVP under consideration or equivalently that $-k^2$ is not an eigenvalue for the Laplace operator in Ω. In these settings the BVP (1) is well posed and our goal is to calculate an approximation of its solution.

Dirichlet BVPs in domains with corners. Without loss of generality, let $\Omega \subset \mathbb{R}^2$ be a bounded domain with one corner, see Fig. 2-right and consider that, in a small neighborhood of the corner point, Γ is composed of two linear segments. We choose the collocation and source point sets $\mathcal{X}_1$ and $\mathcal{Y}$ as in section 2 and approximate the solution of the Dirichlet BVP in Ω by

$$\tilde{u}(x) = \sum_{j=1}^{n} \alpha_j \Phi_k(x - y_j) + \sum_{s=1}^{p} \beta_s \phi_s(r(x),\theta(x)), \quad x \in \bar{\Omega}, \tag{12}$$

i.e. we add p extra shape functions ϕ_s, centered at the corner's tip O, to the standard MFS approximation. The pair $(r(x), \theta(x))$ represents the polar coordinates of $x \in \bar{\Omega}$. Accordingly, let (r_i, θ_i) be the polar coordinates of the collocation point $x_i \in \mathcal{X}_1$. Then the enriched method requires the calculation of the unknown coefficients $\boldsymbol{\alpha}$ and $\boldsymbol{\beta} = (\beta_1, \ldots, \beta_p)$ such that $\tilde{u}$ satisfies (approximately) the Dirichlet boundary condition g_1 on the discrete point set $\mathcal{X}_1 \subset \Gamma$.

In matrix form, the resulting $m_1 \times (n+p)$ collocation linear system is

$$\left[\begin{array}{c|c} & \\ \mathbf{A}_1 & \mathbf{B}_1 \\ & \end{array}\right] \left[\begin{array}{c} \boldsymbol{\alpha} \\ - \\ \boldsymbol{\beta} \end{array}\right] = \left[\begin{array}{c} \\ \boldsymbol{g}_1 \\ \\ \end{array}\right], \tag{13}$$

where $\mathbf{A}_1$, $\boldsymbol{g}_1$ and $\boldsymbol{\alpha}$ are defined as in section 2 and the matrix block corresponding to the corner adapted particular solutions is

$$\mathbf{B}_1 = [\phi_s(r_i, \theta_i)]_{m_1 \times p} \tag{14}$$

We will consider $m_1 > n + p$ and the over-determined linear system (13) will be solved in the least squares sense. A TSVD regularization will be used, whenever appropriate.

For a domain Ω with several corners, e.g. a polygon, the generalization of the enriched MFS is straightforward. An extra block of type (14) is appended to the MFS collocation matrix for each additional corner.

Neumann BVPs in domains with corners. Replacing ϕ_s by ψ_s in the approximation (12) and collocating the normal derivative of $\tilde{u}$, on a finite point set $\mathcal{X}_2 \subset \Gamma$, the corresponding $m_2 \times (n+p)$ linear system becomes

$$\left[\begin{array}{c|c} & \\ \mathbf{A}_2 & \mathbf{C}_1 \\ & \end{array}\right] \left[\begin{array}{c} \boldsymbol{\alpha} \\ - \\ \boldsymbol{\beta} \end{array}\right] = \left[\begin{array}{c} \\ \boldsymbol{g}_2 \\ \\ \end{array}\right], \tag{15}$$

where $\mathbf{A}_2$ and $\boldsymbol{g}_2$ are defined as in section 2 and the matrix block $\mathbf{C}_1$ is given by

$$\mathbf{C}_1 = [\partial_\nu \psi_s(r_i, \theta_i)]_{m_2 \times p}\,. \tag{16}$$

For a domain Ω with several corners, e.g. a polygon, the generalization of the enriched MFS is straightforward. Of course, we should avoid choosing collocation points on the tips of the corners, where the normal derivative is not defined.

Dirichlet-Neumann BVPs in domains with corners. For the domain with one corner shown in Fig. 2-right let $C \in \Gamma$ (with $C \neq O$) be the point that divides the boundary into two parts Γ_1 and Γ_2. We approximate the solution of the BVP by

$$\tilde{u}(x) = \sum_{j=1}^{n} \alpha_j \Phi_k(x - y_j) + \sum_{s=1}^{p} \beta_s \varphi_s(r(x), \theta(x)), \quad x \in \bar{\Omega} \tag{17}$$

and the unknown coefficients $\boldsymbol{\alpha}$ and $\boldsymbol{\beta}$ are calculated by imposing the Dirichlet BC g_1 on the point set $\mathcal{X}_1 \subset \Gamma_1$ and the Neumann BC g_2 on the point set $\mathcal{X}_2 \subset \Gamma_2$. In matrix form we have to solve the following $m \times (n+p)$ linear system

$$\left[\begin{array}{c|c} \mathbf{A}_1 & \mathbf{D}_1 \\ -- & -- \\ \mathbf{A}_2 & \mathbf{D}_2 \end{array}\right] \left[\begin{array}{c} \boldsymbol{\alpha} \\ - \\ \boldsymbol{\beta} \end{array}\right] = \left[\begin{array}{c} \boldsymbol{g}_1 \\ - \\ \boldsymbol{g}_2 \end{array}\right], \tag{18}$$

where $\mathbf{A}_1$, $\mathbf{A}_2$, $\boldsymbol{g}_1$ and $\boldsymbol{g}_2$ are defined as in section 2 and the matrix blocks $\mathbf{D}_1$ and $\mathbf{D}_2$ are given by

$$\begin{aligned} \mathbf{D}_1 &= [\varphi_s(r_i, \theta_i)]_{m_1 \times p} \\ \mathbf{D}_2 &= [\partial_\nu \varphi_s(r_i, \theta_i)]_{m_2 \times p}\,. \end{aligned} \tag{19}$$

Dirichlet BVPs in domains with cracks. In the limit case, when the interior angle at the corner is 2π (with $\omega = 1/2$) we may consider the solution of BVPs in domains with cracks. Graphical examples of the corresponding functions

$$\phi_s(r,\theta) = J_{s/2}(kr)\sin(s\theta/2), \quad s \in \mathbb{N}$$

are shown in Fig. 4.

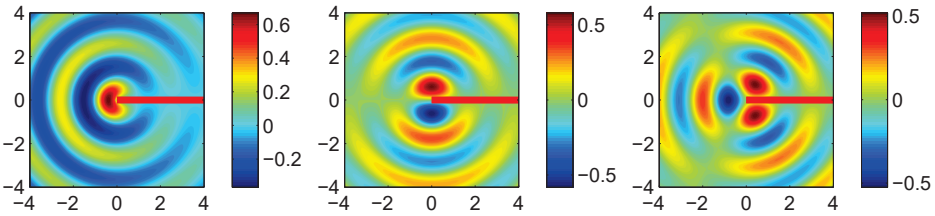

Figure 4: The local behavior of the functions ϕ_s for a domain with a crack, $k = 3,\ s = 1, 2, 3$.

The enriched MFS is applied in the same way as described before, the only difference being that we have to consider an extra set of collocation points on the crack γ. We assume that one of the crack's tips lies on the boundary Γ of the domain, otherwise a domain decomposition technique should be considered. The other tip, i.e. the pole O, is interior to Ω.

From a numerical point of view, the shape functions with even indices $s = 2, 4, 6, \ldots$ are already taken into account by the span of fundamental solutions. We will exclude the corresponding terms from our approximation basis since the same effect may be achieved by taking more source points.

Analyzing the asymptotic behavior of ϕ_s for $r \to 0$ we can verify that these functions exhibit the correct local behavior near the crack's tip O. More precisely, we have

$$J_s(kr) \sim (kr/2)^s / \Gamma(s+1), \quad r \to 0,\ s > 0 \tag{20}$$

where $\Gamma(\cdot)$ is the Gamma functions, see [1]. Consequently, for $r \to 0$, the extra span of corner adapted shape functions behaves as a power-sine series of the form

$$\sum_{s=1}^{p} a_s r^{s-1/2} \sin((s-1/2)\theta),$$

where $a_s := \beta_s (k/2)^{s-1/2}/\Gamma(s+1/2)$.

The first term ($s = 1$) from this series is the most important as it will produce a jump with a singular first order derivative at the crack's tip O. At the same time this term is continuous in $\bar{\Omega}$. In general, the term of order s will induce a singularity on the solution's derivative of order s while all lower order derivatives will be continuous and null across the crack's tip. Of course, the remaining span of fundamental solutions will take care of non zero boundary conditions at the tip O.

4.2. The resonance case - eigenproblems for the Laplace operator

In the resonance case, we search for frequencies $k > 0$ for which there exists a non-trivial solution u, known as an eigenfunction, of the BVP (1) with homogeneous boundary conditions $g_1 = g_2 = 0$. Such frequencies are called eigenfrequencies and they depend on the geometry of the domain Ω.

Dirichlet eigenfrequencies. We will describe the formulation of the enriched MFS for the calculation of Dirichlet eigenfrequencies in domains with corners. The case of domains with cracks that intersect the boundary may be treated analogously. The Subspace Angle Technique (SAT) introduced in [9] will be applied here.

Consider, as before, the sets of boundary collocation and source points $\mathcal{X}_1$ and $\mathcal{Y}$ and let $\mathcal{Z}$ be a set of q randomly distributed domain points z_i

$$\mathcal{Z} = \{z_i \in \Omega : \ i = 1, \ldots, q\}.$$

We define the following $(m_1 + q) \times (n + p)$ matrix that depends on the frequency k

$$\mathbf{A}(k) = \left[\begin{array}{c|c} \mathbf{A}_1(k) & \mathbf{B}_1(k) \\ --- & --- \\ \mathbf{A}_3(k) & \mathbf{B}_2(k) \end{array} \right], \tag{21}$$

with $\mathbf{A}_1$ and $\mathbf{B}_1$ defined as before and

$$\mathbf{A}_3(k) = [\Phi_k(z_i - y_j)]_{q \times n} \tag{22}$$

$$\mathbf{B}_2(k) = [\phi_s(r_i^z, \theta_i^z)]_{q \times p}\,. \tag{23}$$

Here (r_i^z, θ_i^z) are the polar coordinates of the domain knot z_i. Next, we calculate a QR factorization of $\mathbf{A}(k)$ and obtain the matrix

$$\mathbf{Q}(k) = \left[\begin{array}{c} \mathbf{Q}_1(k) \\ ---- \\ \mathbf{Q}_2(k) \end{array} \right]_{(m_1+q)\times(n+p)} \tag{24}$$

where $\mathbf{Q}_1(k)$ is a $m_1 \times (n + p)$ block corresponding to the boundary collocation points and $\mathbf{Q}_2(k)$ is a $q \times (n + p)$ block associated with the domain points. To obtain approximations for the eigenfrequencies we study the variation of the smallest singular value of the matrix $\mathbf{Q}_1(k)$, which we denote by $\sigma(k)$, as a function of k. If $\sigma(k) \approx 0$, then we have a good approximation for the eigenfrequency (see [9] for details). To search for the frequencies where the minimum of $\sigma(k)$ is attained we use an algorithm based on the golden ratio search method, e.g. [3].

Neumann eigenfrequencies. The approach for the calculation of the Neumann eigenfrequencies is similar to the Dirichlet case. The corresponding $(m_2 + q) \times (n + p)$ matrix is

$$\mathbf{A}(k) = \left[\begin{array}{c|c} \mathbf{A}_2(k) & \mathbf{C}_1(k) \\ --- & --- \\ \mathbf{A}_3(k) & \mathbf{C}_2(k) \end{array} \right] \tag{25}$$

with $\mathbf{A}_2,\ \mathbf{A}_3,\ \mathbf{C}_1$ defined respectively in (5), (22), (16) and

$$\mathbf{C}_2(k) = [\psi_s(r_i^z, \theta_i^z)]_{q \times p}. \tag{26}$$

Dirichlet-Neumann eigenfrequencies. The algorithm for the calculation of the eigenfrequencies in the case of mixed boundary conditions is a combination of the previous two approaches. Here, the $(m + q) \times (n + p)$ matrix $\mathbf{A}(k)$ is

$$\mathbf{A}(k) = \left[\begin{array}{c|c} \mathbf{A}_1(k) & \mathbf{D}_1(k) \\ --- & --- \\ \mathbf{A}_2(k) & \mathbf{D}_2(k) \\ --- & --- \\ \mathbf{A}_3(k) & \mathbf{D}_3(k) \end{array} \right] \tag{27}$$

with $\mathbf{A}_1,\ \mathbf{A}_2,\ \mathbf{A}_3,\ \mathbf{D}_1,\ \mathbf{D}_2$ defined as before and

$$\mathbf{D}_3(k) = [\varphi_s(r_i^z, \theta_i^z)]_{q \times p}. \tag{28}$$

5. Numerical simulations

Several numerical examples will be presented in this section in order to illustrate the high accuracy of the enriched MFS technique. BVPs with Dirichlet and mixed Dirichlet-Neumann boundary conditions, posed in simply and multiply connected domains with corners and cracks will be solved in the resonance and non resonance cases.

Since the BVPs are well posed, the quality of the approximate solutions $\tilde{u}$ will be analyzed by measuring the error $u-\tilde{u}$ on the boundary of the domain. Two discrete error norms will be employed for this purpose, namely the maximum norm, with the corresponding maximum absolute error defined as

$$\varepsilon_\infty := \max_{t\in\mathcal{T}} |u(t)-\tilde{u}(t)| \tag{29}$$

and the discrete $L^2(\Gamma)$ norm, with the corresponding RMS error

$$\varepsilon_2 := \left(\frac{1}{\#\mathcal{T}}\sum_{t\in\mathcal{T}} |u(t)-\tilde{u}(t)|^2\right)^{1/2}. \tag{30}$$

In both cases $\mathcal{T}\subset\Gamma$ represents a finite set of error test points. Additionally, the corresponding relative absolute and relative RMS errors are defined by

$$\varepsilon_\infty^{rel} := \frac{\max_{t\in\mathcal{T}}|u(t)-\tilde{u}(t)|}{\max_{t\in\mathcal{T}}|u(t)|} \quad \text{and} \quad \varepsilon_2^{rel} := \left(\frac{\sum_{t\in\mathcal{T}}|u(t)-\tilde{u}(t)|^2}{\sum_{t\in\mathcal{T}}|u(t)|^2}\right)^{1/2}.$$

In the resonance case, we will also use the maximum norm (29), in order to analyze the quality of the eigenfrequency approximation. More precisely, based on results presented by Moler and Payne, cf. [35], it is possible to obtain *a posteriori* bounds for the error of the eigenfrequency in terms of the magnitude of the approximated eigenfunction on the boundary, e.g. [9, 3].

For the solution of the linear systems involving ill-conditioned matrices we considered the TSVD regularization technique, e.g. [24]. In particular, the default cut-off parameter $\epsilon_{mch}\max(m,n)||\mathbf{A}||_2$ of the Matlab's backslash routine was used. Here $\epsilon_{mch}\approx 10^{-16}$ represents the machine precision in double precision computation.

5.1. The non-resonance case

From an application's point of view we will consider the solution of direct, interior scattering problems. A problem of this type consists in computing the scattered wave field u^{sc} generated from the interaction between a known incident field u^{inc} and an obstacle of known properties. In acoustics, the interior problem may simulate, for example, the measurement of the sound field produced by an interior source (e.g. a speaker) inside a closed room [6]. Impenetrable, sound-soft or sound-hard boundaries will be simulated here. In the first case, the pressure of the total wave $u^{tot}=u^{sc}+u^{inc}$ vanishes on the boundary and a Dirichlet BVP is solved for u^{sc}, subjected to the boundary condition $g_1=u^{sc}=-u^{inc}$. In the second case the normal velocity $\partial_\nu u^{tot}$ vanishes and a Neumann BVP is solved with $g_2=\partial_\nu u^{sc}=-\partial_\nu u^{inc}$.

We will focus on the solution of BVPs with boundary conditions generated by spherical incident waves with singularities (source points) located inside the domain of interest. The accuracy of the standard MFS is unsatisfactory for such problems, and as we will illustrate in the examples below, the enriched MFS leads to a significant improvement of the numerical results.

A benchmark example.

In order to validate the numerical algorithm we considered the Motz's Helmholtz problem, posed in the rectangular domain $\Omega=(-1,1)\times(0,1)$, see Fig. 5-left. The numerical results by the enriched MFS were compared with the results presented in [32], where a Trefftz method using piecewise particular solutions was applied. The same benchmark example will be considered later on, in section 5.2, for the resonance case.

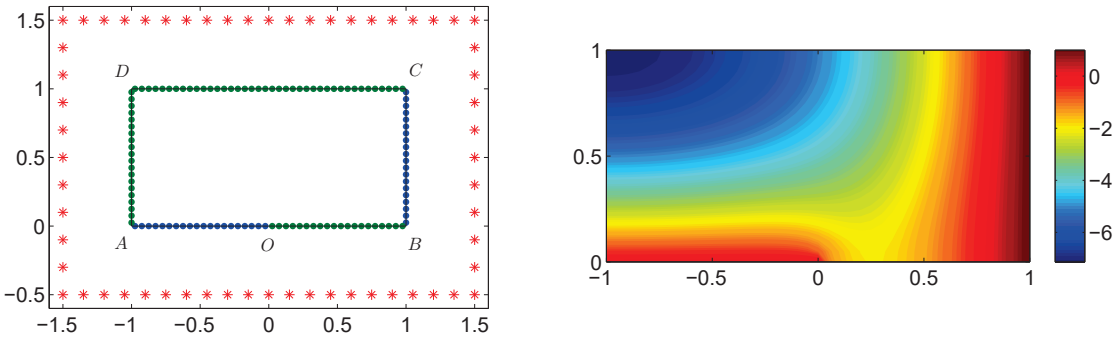

Figure 5: The collocation and source points for the Motz's Helmholtz problem (left) and the real part of the approximate solution for $k = \sqrt{3}$ (right).

The following mixed Dirichlet-Neumann boundary conditions were imposed on Γ

$$\begin{cases} u = 0 & \text{on} \quad \overline{AO} \\ u = 1 & \text{on} \quad \overline{BC} \\ \partial_\nu u = 0 & \text{on} \quad \overline{OB} \cup \overline{CD} \cup \overline{DA} \end{cases} \tag{31}$$

and we tested our method with $k = \sqrt{3}$ and $n = 180$ equally-spaced source points, located on the boundary of the larger rectangle $(-1.5, 1.5) \times (-0.5, 1.5)$. For the boundary collocation points we took $m_1 = 120$ and $m_2 = 240$ uniformly distributed knots on Γ_1 and Γ_2, respectively.

The standard MFS showed unsatisfactory results for this knot configuration. RMS errors of order $O(10^{-2})$ were measured on the boundary Γ. In particular, the maximum of the absolute error was observed at the origin, which is also the only singular point of the exact solution. This behavior may be explained, from an analytical point of view, by studying the regularity of the shape functions ψ_s and φ_s, corresponding to the corners A, B, C, D and O. At the origin (where $\omega = 1$) we have $(s - 1/2)\omega \notin \mathbb{N}$ and therefore the shape functions φ_s are singular, due to the singularity of the Bessel functions $J_{(s-1/2)\omega}$, see (20). On the other hand, at the remaining corners (where $\omega = 2$) the orders $s\omega$ and $(s-1/2)\omega$ of the Bessel functions are integer and thus ψ_s and φ_s are regular functions. As a consequence, only the extra shape functions corresponding to the origin will improve the approximation qualities of the MFS basis, also see Remark 2. No shape functions will be added for the rest of the corners since the same effect may be achieved by increasing the number of source points.

In Table 1 we presented the numerical results by the enriched MFS, for several values of the number p of extra shape functions. The results in the first row corresponds to the standard MFS, i.e. when no augmentation of the basis is performed.

p	ε_2 on Γ_1	ε_2 on Γ_2
0	$9.05e-02$	$3.64e-02$
1	$1.85e-03$	$1.45e-03$
2	$6.06e-06$	$4.09e-06$
3	$4.34e-08$	$3.95e-08$
4	$8.46e-10$	$1.18e-09$
5	$1.37e-11$	$1.36e-11$
6	$9.69e-15$	$1.94e-14$

Table 1: The boundary error for the Motz's Helmholtz problem with $k = \sqrt{3}$.

The values of the RMS errors indicate that by adding just 5 extra shape functions we can achieve the accuracy of the best results presented in [32]. Furthermore, with $p = 6$ the maximum available machine

precision is exhausted. Numerical errors as low as $O(10^{-15})$ were observed, which corresponds to an improvement of approximately 4 orders of magnitude over the results presented in [32]. A plot of the real part of the approximate solution is shown in Fig. 5-right.

A Dirichlet BVP in a polygonal domain.

Consider a vertical cross-section of a room, see Fig. 6-left, with a speaker located at $S = (3, 5)$. Assume that the walls of the room are sound-soft and that the speaker may be represented by a spherical wave with frequency $k = 2$. We intend to reconstruct the scattered wave pattern inside the room Ω.

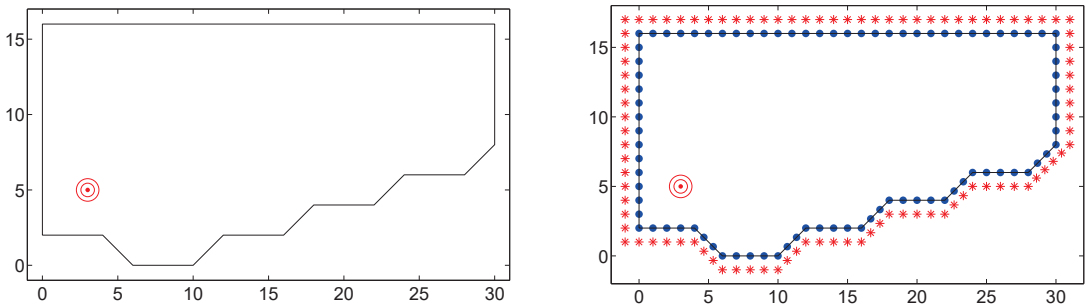

Figure 6: The geometry of the room Ω (left) and the collocation and source points for the MFS (right).

Mathematically, this problem is modelled by a Dirichlet BVP for the Helmholtz equation. For the incident field we chose the spherical wave

$$u^{inc}(x) = Y_0(k|x - S|), \quad x \in \Gamma$$

and our goal is to calculate the scattered wave u^{sc} in Ω. Note that the boundary data is generated by the imaginary part of a fundamental solution with singularity lying inside the domain and thus the exact solution of the BVP is not known. We will measure the error of $\tilde{u}^{sc}$ on Γ.

This example was analyzed in [5] where the standard MFS was applied. The best numerical results that were reported correspond to $\varepsilon_\infty^{rel} \approx 3.5\%$, with the MFS showing serious difficulties in approximating the solution near the corners at the base of the room. Source points extremely close to the non convex corners were considered but the numerical results remained unsatisfactory. This problem is due to the difference in the solution's and the trial singularities' nature. Next, we apply the enriched MFS method.

Since the particular solutions $\phi_s(r, \theta)$ will take care of the singular behavior of the scattered wave at the corners we may consider an arbitrary (admissible) pseudo boundary $\hat{\Gamma}$. A standard choice is a boundary $\hat{\Gamma}$ that resembles the domain's boundary, see Fig. 6-right. Denote by δ the distance between the corresponding parallel sections of Γ and $\hat{\Gamma}$. The collocation (source) points will be equally spaced on Γ (respectively, on $\hat{\Gamma}$).

We took the same $m = 865$ collocation points on Γ as in [5] and $n = 454$ source points on $\hat{\Gamma}$ with $\delta = 0.5$. For this knot configuration the maximum absolute error by the standard MFS, measured on 4310 boundary knots, was $\varepsilon_\infty = 0.068$. Next, we enriched the MFS basis with $p = 10$ extra particular solutions ϕ_s for each of the singular corners, see Remark 2. The absolute error, as a function of the boundary's arc-length (starting from $(0, 2)$ in counter-clockwise direction), is shown in Fig. 7-left. All linear systems were solved by TSVD regularization since the corresponding matrices were ill-conditioned.

By the enriched MFS method, we measured a maximum error of $\varepsilon_\infty = 1.545e-7$ which corresponds to $\varepsilon_\infty^{rel} \approx 5.150e-7$, since we have $\max_\Gamma |g_1| \approx 0.3$. The same 4310 error test knots on Γ were used. Comparing with the numerical results from [5] we observed an improvement of approximately 5 orders of magnitude in terms of the boundary relative error. The pattern of the scattered wave in Ω is illustrated in Fig. 7-right.

We conclude this example by analyzing the influence of the number p of extra shape functions (per singular corner) on the method's accuracy, see Table 2. The case $p = 0$ corresponds to the standard MFS.

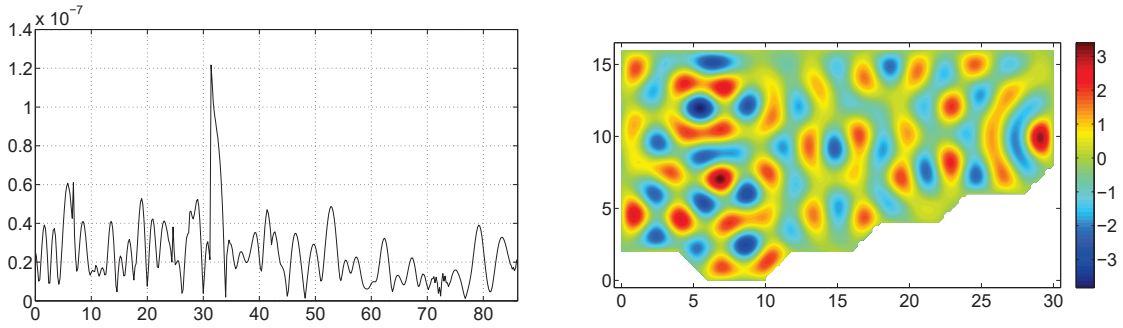

Figure 7: The absolute error on Γ (left) and the real part of the scattered wave in Ω (right).

p	ε_∞	ε_2	ε_2^{rel}	$Cond_2(\mathbf{A})$
0	$6.80e-2$	$3.86e-3$	$3.06e-2$	$3.6e+08$
1	$1.82e-2$	$1.80e-3$	$1.42e-2$	$3.6e+08$
2	$6.11e-4$	$5.55e-5$	$4.40e-4$	$3.6e+08$
3	$6.64e-5$	$3.04e-6$	$2.40e-5$	$3.9e+08$
5	$5.84e-7$	$6.06e-8$	$4.80e-7$	$2.4e+09$
10	$1.55e-7$	$3.08e-8$	$2.44e-7$	$3.9e+11$
15	$9.31e-7$	$3.62e-7$	$2.87e-6$	$2.7e+15$

Table 2: The boundary error for several values of p. ($n = 454,\ m = 865,\ k = 2,\ \delta = 0.5$)

The numerical results indicate that by adding just two particular solutions per corner we can decrease the absolute MFS error by two orders of magnitude. The relative error of the resulting approximation is $\varepsilon_\infty^{rel} \approx 0.2\%$ which, in most cases, is sufficient for practical purposes. In the last column we included the values of the condition number of the corresponding collocation matrix. Similar to the standard MFS [10], the improvement of the approximation is limited by the conditioning of the linear system. More precisely, the method becomes unstable as soon as $1/Cond_2(\mathbf{A})$ reaches the maximum allowed machine precision ϵ_{mch}.

A Dirichlet-Neumann BVP in a multiply-connected domain with corners.

A BVP with mixed Dirichlet-Neumann boundary conditions is analyzed here. For the domain Ω we took a horizontal cross-section of a room with two interior columns, see Fig. 8-left. The columns have a circular cross-section with a unitary radius and centers $(4, 6)$ and $(16, 6)$. One of the rooms's walls is defined through a semi-ellipse with axis $(10, 6)$ and center $(10, 6)$ and the remaining walls are plane. An example of the collocation and source points is shown in Fig. 8-right. The collocation and source points for the columns are equally spaced.

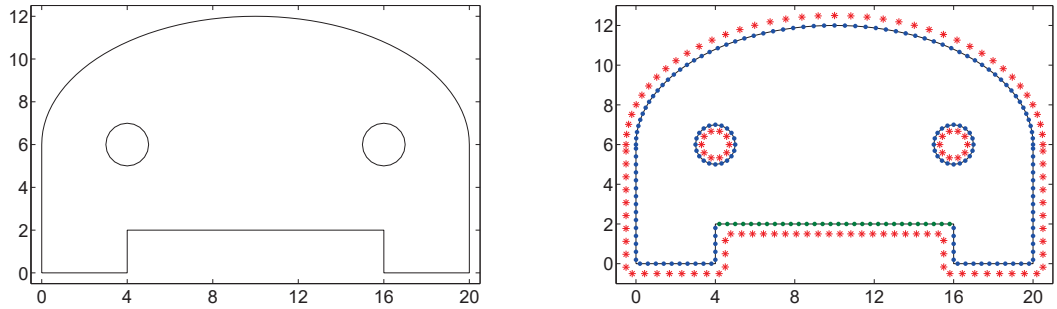

Figure 8: The domain Ω (left) and collocation and source points (right).

Assume that the wall $\Gamma_2 := \{x \in \Gamma :\ 4 < x_1 < 16,\ x_2 = 2\}$ is sound-hard (Neumann BC) and the rest of the boundary ($\Gamma_1 := \Gamma \backslash \Gamma_2$) is sound-soft (Dirichlet BC). Consider two speakers, located at $S_1 = (2, 1)$ and $S_2 = (18, 1)$, both with a (real) unitary amplitude. The boundary data is defined in terms of the incident wave

$$u^{inc}(x) = Y_0(k|x - S_1|) + Y_0(k|x - S_2|),$$

and the pseudo boundary was chosen to resemble Γ, see Fig. 8-right. Taking $m_1 = 681$, $m_2 = 120$, $n = 401$ and $k = 1$ the standard MFS showed a relative error $\varepsilon_\infty^{rel} = 35\%$ on Γ_1 and $\varepsilon_\infty^{rel} = 292\%$ on Γ_2. Clearly these results are unsatisfactory. The main error accumulation occurs near the critical points $(4, 2)$ and $(16, 2)$, showing the difficulty of the MFS to approximate the solution near those (singular) corners. The linear system was solved by TSVD regularization.

In order to improve the accuracy of the method we augmented the MFS basis by $p = 20$ corner adapted shape functions φ_s for each of the two problematic corners. With this modification, we measured $\varepsilon_\infty^{rel} = 9.28e - 5$ on Γ_1 and $\varepsilon_\infty^{rel} = 8.31e - 5$ on Γ_2 which corresponds to a decrease of approximately 4 orders of magnitude, in comparison with the results from the standard MFS. The plot of the real part of the scattered wave is shown in Fig. 9-left. As expected, the imaginary part of the scattered wave is close to zero since the boundary data is real. The values of the error were measured taking into account the total, complex valued, scattered wave.

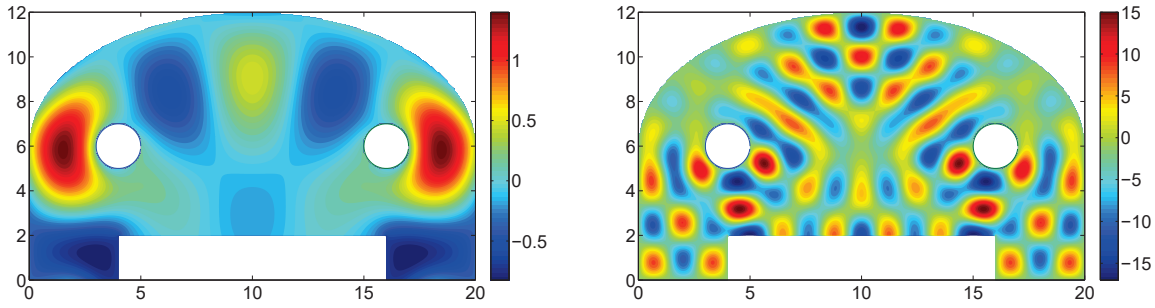

Figure 9: The scattered wave in $\bar{\Omega}$ for $k = 1$ (left) and $k = 3$ (right).

In Fig. 9-right we included the plot of the scattered wave with $k = 3$, $p = 30$, $m_1 = 1361$, $m_2 = 240$ and $n = 801$. Here the relative errors were $\varepsilon_\infty^{rel} = 7.96e - 4$ on Γ_1 and $\varepsilon_\infty^{rel} = 4.03e - 6$ on Γ_2.

A Dirichlet BVP for a domain with crack.

Consider the analytic domain $\Omega \subset \mathbb{R}^2$, bounded by the closed parametric curve

$$\Gamma := \{x = (4\cos(t) + 0.3\cos(-4t), 4\sin(t) + 0.3\sin(-4t)) :\ t \in [0, 2\pi]\}.$$

Let γ be a linear crack of Ω with end points $A = (2, 0)$ and $B \in \Gamma$. The point B corresponds to $t = 0$ in the boundary parametrization, see Fig. 10-left.

An example of the distribution of the collocation points on the boundary (m_Γ points) and on the crack (m_γ points) and of the source points on $\hat{\Gamma} := \mu \times \Gamma$ ($\mu > 1$) are shown in Fig. 10-right. For the BVP we will consider the interior scattering problem in $\Omega \backslash \bar{\gamma}$ for a spherical incident wave with source point located at $S = (1, -3) \in \Omega$

$$u^{inc}(x) = Y_0(k|x - S|).$$

Assuming that the boundary and the crack are sound-soft, the Dirichlet BC is given by $g_1 = -u^{inc}$ on $\Gamma \cup \gamma$. From a physical point of view the crack may be seen as an interior sound-soft wall with neglectable thickness.

Tests were performed for several choices of collocation/source points and pseudo boundaries, but the standard MFS showed no convergence for this problem. The best numerical results for $k = 1$ were $\varepsilon_\infty^{rel} \approx 30\%$ on the boundary Γ and $\varepsilon_\infty^{rel} \approx 10\%$ on the crack γ. For the following simulations we applied the enriched MFS.

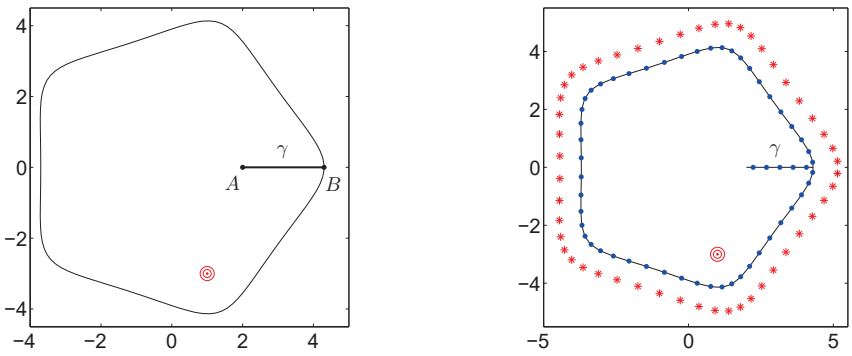

Figure 10: The domain Ω (left) and the collocation and source points (right).

Varying the number of collocation and source points. In Table 3 we include the numerical results from the enriched MFS with $k = 1$. A fixed pseudo boundary with $\mu = 1.2$ was considered for these simulations. TSVD regularization was used for the solution of the corresponding linear systems. The error was measured on $5m_\Gamma$ and $5m_\gamma$ error test points on Γ and on γ, respectively.

m_Γ	m_γ	n	p	ε_∞ on Γ	ε_∞ on γ	$Cond_2(\mathbf{A})$
150	50	75	2	$4.48e-3$	$2.09e-2$	$2.3e+05$
200	75	100	4	$1.14e-4$	$1.03e-4$	$1.1e+07$
250	100	125	6	$9.13e-7$	$8.14e-7$	$4.5e+08$
300	125	150	8	$1.71e-8$	$3.47e-8$	$1.9e+10$

Table 3: The error ε_∞ of $\tilde{u}^{sc}$ on Γ and γ for several knot configurations and values of p.

The enrichment technique led to an improvement of the MFS results by 7 orders of magnitude with just 8 extra shape functions. The corresponding relative errors were of the same order of magnitude since we have $\max_\Gamma |g_1| = 0.52$ and $\max_\gamma |g_1| = 0.32$ for this example. The values of the condition number of the linear systems indicate that further improvement of the numerical results is still possible by increasing the number of knots and extra shape functions. No significant error accumulation was observed near the tips of the crack, see Fig. 11.

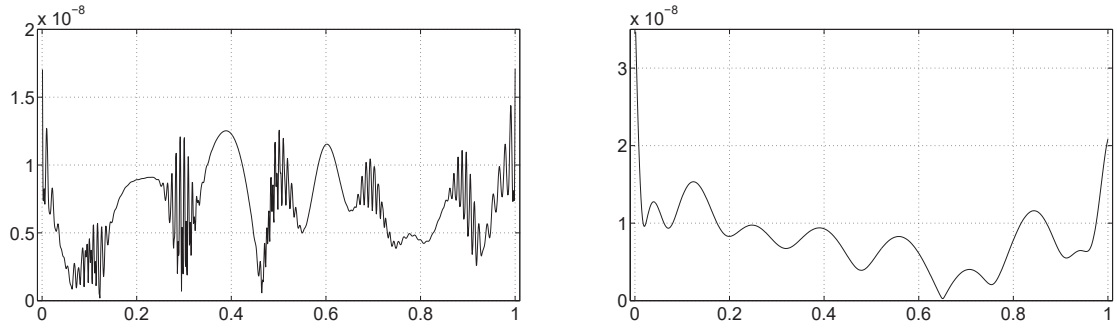

Figure 11: The absolute error on Γ (left) and on γ (right). $m_\Gamma = 300,\ m_\gamma = 125,\ n = 150,\ p = 8$.

Varying the length of the crack. Previous studies, involving domains with cracks in the field of linear elasticity, indicate that the accuracy of the MFS deteriorates when the length of the crack is increased, e.g. [28, 8].

In order to verify if this is also the case for the MFS variant presented here we conducted several numerical tests, varying the length $|\gamma|$ of the crack, see Table 4. We fixed $k = 2$ and $\mu = 1.2$ for the pseudo boundary $\hat{\Gamma}_\mu$. Our goal was to approximate the solution u^{sc} with an error of order $\varepsilon_\infty = O(10^{-7})$ on $\Gamma \cup \gamma$.

tip A	$\lvert\gamma\rvert$	m_Γ	m_γ	n	p	ε_∞ on Γ	ε_∞ on γ	$Cond_2(\mathbf{A})$
$(3,0)$	1.3	250	20	125	6	$6.03e-7$	$6.85e-7$	$1.8e+08$
$(2,0)$	2.3	250	30	125	8	$2.74e-7$	$5.61e-7$	$1.7e+08$
$(1,0)$	3.3	250	40	125	10	$1.71e-7$	$1.58e-7$	$1.7e+08$
$(0,0)$	4.3	300	50	150	12	$5.09e-7$	$6.07e-7$	$7.1e+09$
$(-1,0)$	5.3	300	60	150	14	$1.44e-7$	$2.54e-7$	$7.1e+09$
$(-2,0)$	6.3	300	70	150	16	$1.82e-7$	$3.71e-7$	$8.2e+10$
$(-3,0)$	7.3	350	80	175	20	$6.65e-7$	$6.55e-7$	$1.5e+14$

Table 4: The error ε_∞ of $\tilde{u}^{sc}$ on Γ and γ for several values of the crack's length. $k = 2,\ \mu = 1.2$.

From the numerical results in Table 4 we may conclude that the achievable precision of the enriched MFS does not depend on the length of the crack. Highly accurate results were obtained by increasing the number m_γ of collocation points on the crack and the number of extra shape functions. Approximately 15 extra collocation points per unit increase in the crack's length and 2 extra shape functions were sufficient in order to reach the desired precision. A minor increase in the number of sources and boundary collocation points was also necessary in the cases when $|\gamma| > \text{diam}(\Omega)/2$.[1] The values of the condition number of the linear systems indicate that further improvement of the results is still possible for reasonable length cracks. For example, numerical errors of order 10^{-10} were observed for $A = (2,0)$.

In Fig. 12 we included the graphical results for a short crack, medium length crack and a long crack. The absolute value of the total wave u^{tot} was plotted, for the corresponding knot configurations from Table 4. Note that, since sound-soft walls were simulated, u^{tot} is null on the boundary and on the crack. As expected from a physical point of view, for $A = (-3,0)$, the crack acts like a barrier, obstructing the wave propagation in the upper half of the room.

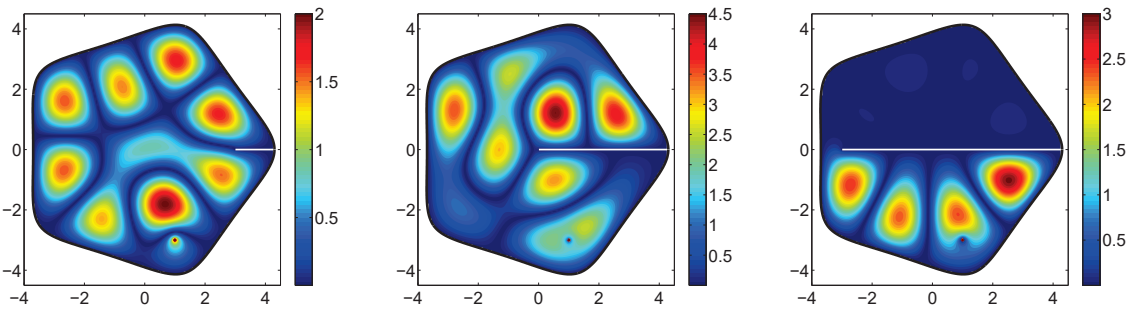

Figure 12: The absolute value of the total wave $u^{tot} = u^{sc} + u^{inc}$ for $A = (3,0)$, $A = (0,0)$ and $A = (-3,0)$. $k = 2,\ \mu = 1.2$.

Varying the value of the frequency k. The real part of the scattered wave for $k = 1, 5, 10$ is shown in Fig. 13. In the three cases we increased the values of m_Γ, m_γ, n and p until an error of order $\varepsilon_\infty^{rel} = O(10^{-5})$ was achieved on $\Gamma \cup \gamma$, i.e. the three approximations have less than 0.01% of relative error. Here, the interior tip of the crack is $A = (2,0)$.

5.2. The resonance case

The eigenvalue problems for PDEs generally arise in the context of vibration or resonance. For example the eigenfrequencies $k > 0$ of a planar domain Ω may be viewed as the resonance frequencies of a drum with

[1] Here $\text{diam}(\Omega)$ denotes the diameter of the domain, i.e. $\text{diam}(\Omega) = \max\{|x - y| : x, y \in \Omega\}$.

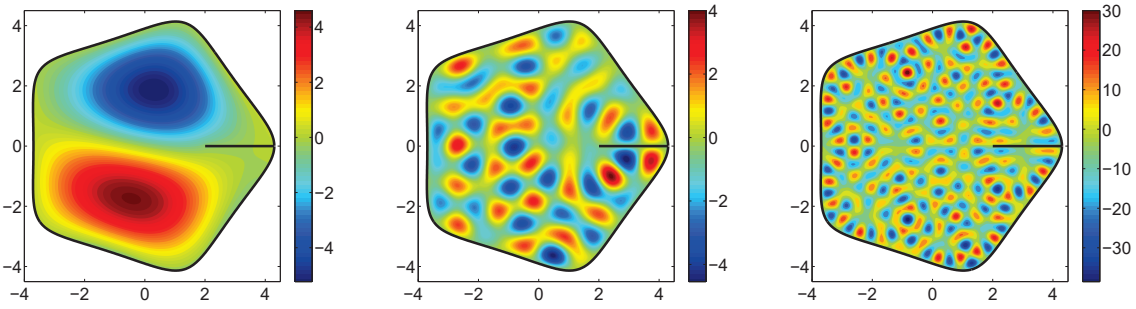

Figure 13: The real part of the scattered wave u^{sc} for $k = 1, 5, 10$.

shape defined by the region Ω. The associated eigenfunctions represent the displacement of the vibrating membrane. We will focus on the numerical calculation of the eigenfrequencies for non-smooth domains and present three examples which illustrate the high accuracy of the proposed enriched MFS.

A circular domain with crack.

For the first example we will consider a circular domain with a crack. The corresponding Dirichlet eigenproblem has been addressed by several authors in the past, see [13, 14]. In particular, the standard MFS, coupled with a domain decomposition technique has been applied in [14]. However, the procedure proposed in the referred publication does not take into account the derivative's discontinuity that generally occurs at the interior tip of the crack and the reported results have low accuracy. In the following we apply the enriched MFS.

Let Ω be the unitary disk (centered at the origin) with a crack γ, defined through its end points $A = (1, 0)$ and $B = (1 - a, 0)$, for $a \in]0, 2[$. For $a = 0.4$ we took $p = 6$ particular solutions ϕ_s centered at the crack's tip $B = (0.6, 0)$. Also, we selected $n = 30$ source points on $\hat{\Gamma} = 1.5 \times \Gamma$, $m = 80$ collocation points on Γ and $q = 20$ interior points, randomly distributed in Ω, see Fig. 14-left.

In Figure 14-right we plotted $\sigma(k)$ as a function of $k \in (0, 6)$. The points of the graph where $\sigma(k) \approx 0$ correspond to the approximated values of the eigenfrequencies.

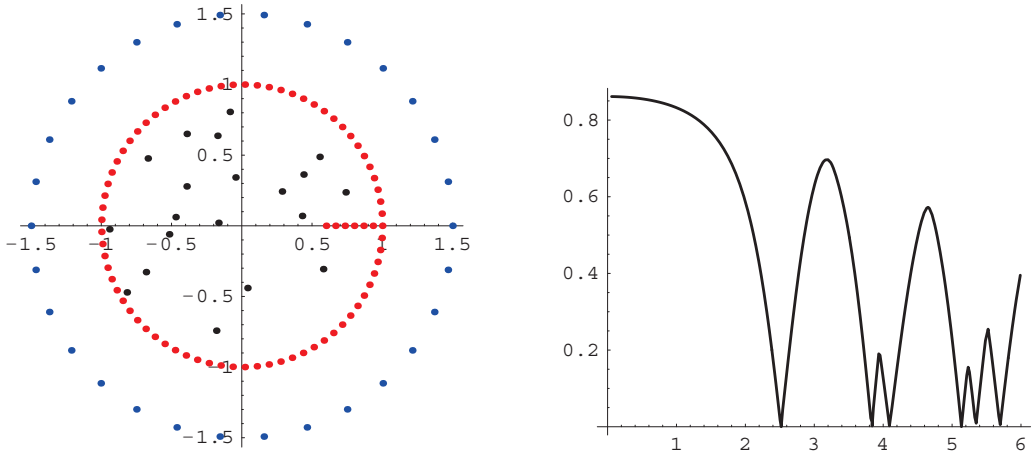

Figure 14: The collocation, source and interior points (left) and $\sigma(k)$ as a function of $k \in (0, 6)$ (right).

Varying the number p of extra shape functions. We present convergence results for the first eigenfrequency k_1, calculated with $n = 50$, $m = 170$ and several values of the parameter p. In Fig. 15-left we plotted the

error of k_1 as a function of p. For the 'exact' value of the eigenfrequency we took the approximation $k = 2.514234380868$ obtained with $p = 50$. We believe that all the digits of this value are correct. In Fig. 15-right we plotted $\sigma(k_1)$ as a function of p. For $p = 50$, we obtained $\sigma(k_1) \approx 4.51 \times 10^{-13}$.

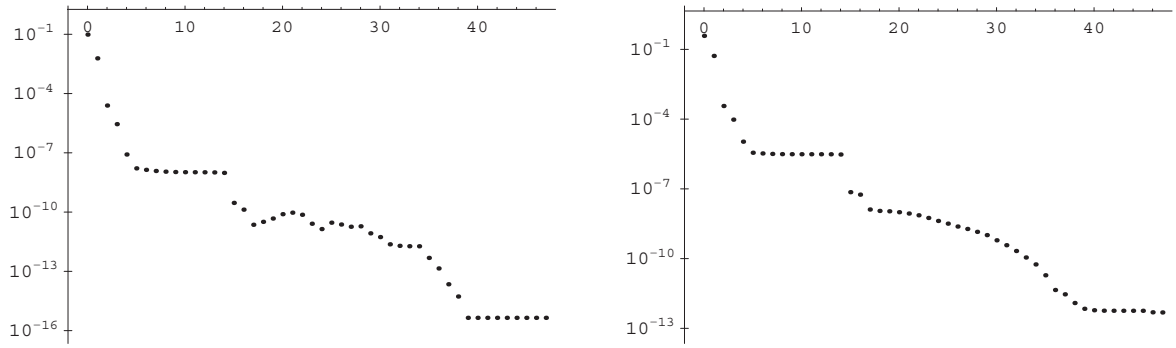

Figure 15: The absolute error of k_1 as a function of p (left) and $\sigma(k_1)$ as a function of p (right).

The eigenfunction corresponding to the eigenfrequency k_1 is represented in Fig. 16-left. Additionally, the eigenfunctions associated with two higher eigenfrequencies, $k \approx 20.818107405029$ and $k \approx 30.371007667117$, were also included in the same figure.

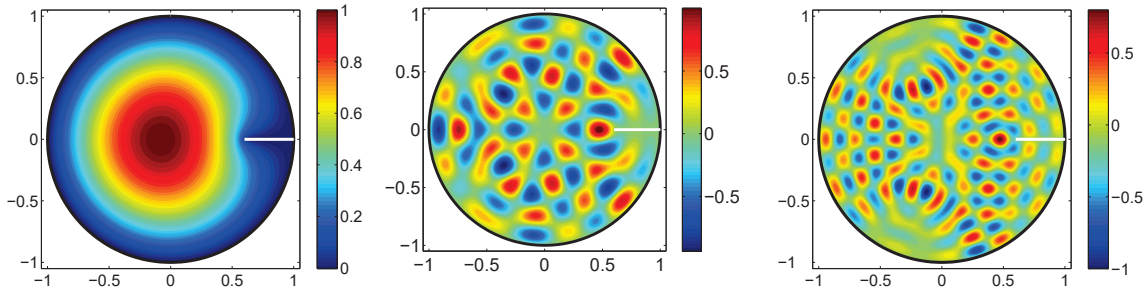

Figure 16: The eigenfunctions associated to three eigenfrequencies of a domain with a crack.

Varying the crack's length a. In Fig. 17 we plotted the smallest six eigenfrequencies as a function of the crack's length a. It is interesting to note that for $a \approx 0.8$ we have a non trivial domain for which the fifth eigenfrequency has multiplicity two.

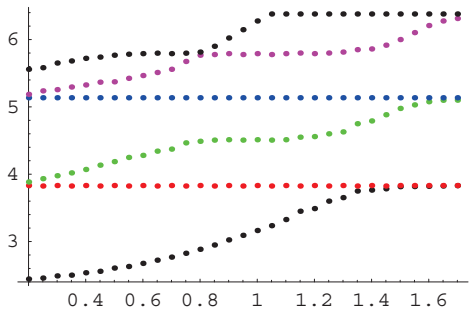

Figure 17: The values of the smallest six eigenfrequencies as a function of a.

A mixed Dirichlet-Neumann eigenproblem in a simply-connected domain.

For the second simulation we will consider the Motz's Helmholtz problem from section 5.1, with homogeneous Dirichlet-Neumann boundary conditions, see Fig. 5-left. Our goal is to calculate approximate values for the first two eigenfrequencies for this problem. We will compare the numerical results from the enriched MFS with the values $k_1 = 1.6630496371$ and $k_2 = 2.6029531186$, calculated with *Mathematica* and presented as correct up to the eleventh significant digit in [32].

The source points for the MFS were uniformly distributed on the boundary of a rectangle $(-2,2)\times(-1,2)$. In Table 5 we present the numerical results for k_1 and k_2 and several knot configurations. As before, augmentation of the MFS basis is only necessary at the origin of the domain.

n	p	k_1	k_2
Li [32]		1.66305	2.60295
Mathematica		1.6630496371	2.6029531186
30	0	1.609659496281966	2.548131236350232
30	3	1.663052202024694	2.602917161213809
80	5	1.663049636796045	2.602953118470179
100	7	1.663049637050797	2.602953118642397
120	8	1.663049637050803	2.602953118643478
140	9	1.663049637050800	2.602953118643468

Table 5: Comparison of the results from Li [32] and the enriched MFS, for the first two eigenfrequencies.

We can observe that all digits of the approximation obtained with $n = 100$ and $p = 7$ coincide with the benchmark values from *Mathematica*. The results suggest that this approximation has (at least) 11 correct digits. Moreover, the last two rows of Table 5 indicate that the corresponding approximations have accuracy close to the machine precision.

A mixed Dirichlet-Neumann eigenproblem in a multiply-connected domain.

For the third simulation we will consider a BVP with mixed Dirichlet-Neumann boundary conditions, posed in a multiply-connected domain. The application of the standard MFS to such problems has been studied in [12] and it has been reported that incorrect spurious eigenfrequencies may occur.

Let Ω be the multiply-connected domain represented in Fig. 18-left. Its boundary is defined by the four curves $C_1 = \{(\cos(t), 3/2\sin(t) - 3/8\cos(3t)\sin(t)) : t \in [0,\pi]\}$, $C_2 = \{0.3(\cos(t),\sin(t)) + (0.3, 0.7) : t \in [0, 2\pi[\}$, $C_3 = \{(x_1, x_2) : x_2 = 0,\ 0 \le x_1 < 1\}$ and $C_4 = \{(x_1, x_2) : x_2 = 0,\ -1 < x_1 < 0\}$. Let $\Gamma_2 := C_4$ and a $\Gamma_1 := C_1 \cup C_2 \cup C_3$. We took $m = 300$ boundary collocation points, $p = 7$ particular shape functions φ_s centered at the origin and $n = 200$ source points selected as in [3], see Fig. 18-right. In order to illustrate the

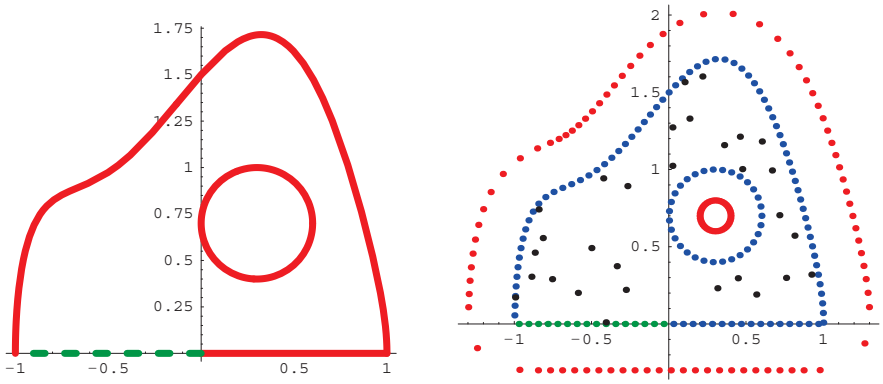

Figure 18: The boundary of a multiply-connected domain with mixed boundary conditions (left) and the collocation, source and interior points (right).

high accuracy of the enriched MFS we analyzed the quality of the approximate eigenfunction $\tilde{u}$ associated to the first eigenfrequency for this domain. In Fig. 19 we plotted the absolute error $|\tilde{u}|$ on C_i, $i = 1, 2, 3$ and $|\partial_\nu \tilde{u}|$ on C_4. The maximum error on the boundary was attained at the origin $x = 0$, and its magnitude was $9.47e-11$ on Γ_1 and $5.16e-10$ on Γ_2.

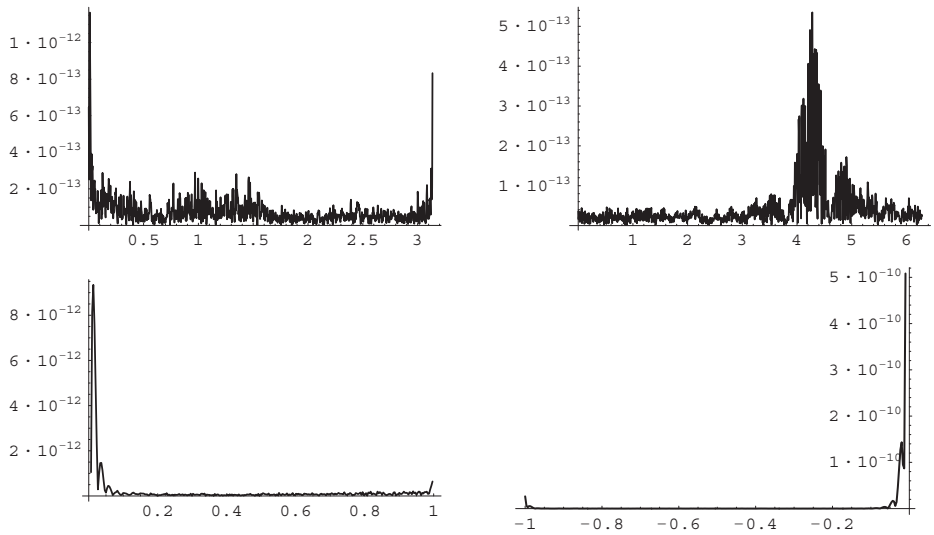

Figure 19: $|\tilde{u}|$ on C_i, i=1,2,3 and $|\partial_\nu \tilde{u}|$ on C_4.

In Fig. 20 we include the density plots of the eigenfunctions associated with the first, third and ninth eigenfrequencies for this domain.

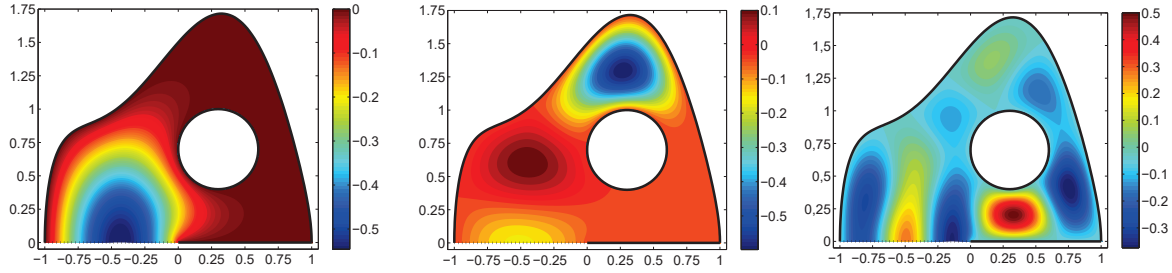

Figure 20: Eigenfunctions associated to the first, third and ninth eigenfrequencies.

6. Concluding remarks

We have developed an enrichment technique for the standard Method of Fundamental Solutions which may be applied for the approximate solution of Helmholtz BVPs with resonance and non-resonance frequencies, posed in domains with corners and cracks. The linearity and the simplicity of implementation of the original method have been preserved, as well as its meshfree and integration free characteristics. The high accuracy of the numerical results presented in section 5 indicate that the developed corner adapted shape functions are appropriate for this type of problems. More precisely, the nature of the solution's singularity at the corner's (crack's) tip is correctly approximated by the trial functions' singularities. The extension of the enrichment technique for non smooth three dimensional domains is under current research.

Acknowledgements. The authors would like to thank Dr. Carlos J. S. Alves for his valuable ideas and many critical discussions concerning the Method os Fundamental Solutions and its variants.

The financial support received from the Fundação para a Ciência e a Tecnologia through the scholarship SFRH/BPD/47595/2008 (first author) and the scientific projects PTDC/MAT/101007/2008 (first author) and PPCDT/MAT/60863/2004, POCTI/MAT/45700/2002 (second author) is also gratefully acknowledged.

References

[1] Abramowitz M. and Stegun I. A., Handbook of Mathematical Functions with Formulas, Graphs, and Mathematical Tables, Dover, 1964.
[2] Alves C. J. S. and Chen C. S., A new method of fundamental solutions applied to nonhomogeneous elliptic problems, Adv Comp Math, 2003; 23:125–142.
[3] Alves C. J. S. and Antunes P. R. S., The Method of Fundamental Solutions applied to the calculation of eigenfrequencies and eigenmodes of 2D simply connected shapes, CMC, 2005; 2(4): 251–266.
[4] Alves C. J. S. and Leitão V. M. A., Crack analysis using an enriched MFS domain decomposition technique, Eng Anal Bound Elem, 2006; 30:160-166.
[5] Alves C. J. S. and Valtchev S. S., Numerical Comparison of two meshfree methods for acoustic wave scattering, Eng Anal Bound Elem, 2005; 29:371–382.
[6] Antonio J., Tadeu A. and Godinho. L., A three-dimensional acoustics model using the method of fundamental solutions, Eng Anal Bound Elem, 2008; 32:525-531.
[7] Barnett A. H. and Betcke T., Stability and convergence of the method of fundamental solutions for Helmholtz problems on analytic domains, Journal of Computational Physics, 2008; 227:70037026.
[8] Berger J. R., Karageorghis A. and Martin P. A., Stress intensity factor computation using the method of fundamental solutons: mixed-mode problems, Int J Numer Meth Engng, 2007; 69:469-483.
[9] Betcke T. and Trefethen L. N., Reviving the Method of Particular Solutions, SIAM Review, 2005; 47:469491.
[10] Bogomolny A., Fundamental solutions method for elliptic boundary value problems, SIAM J. Num. Anal., 1985; 22:644–669.
[11] Chen G. and Zhou J., Boundary Element Method, Academic Press, 1992.
[12] Chen J. T., Chen I. L. and Lee Y. T., Eigensolutions of multiply connected membranes using the Method of Fundamental Solutions, Eng Anal Bound Elem, 2005; 29:166–174.
[13] Chen J. T., Liang M. T., Chen I. L., Chyuan S. W. and Chen K. H., Dual boundary element analysis of wave scattering from singularities, Wave Motion, 1999; 30:367–381.
[14] Chen C. W., Fan C. M., Young D. L., Murugesan K. and Tsai C. C., Eigenanalysis for membranes with stringers using the Method of Fundamental Solutions and domain decomposition, CMES, 2005; 8(1):29–44.
[15] Colton D., Kress R., Inverse Acoustic and Electromagnetic Scattering Theory, Applied Mathematical Science, vol. 93, Springer-Verlag, Berlin Heidelberg, 2nd. edition, 1998.
[16] Courant D. and Hilbert R., Methods of Mathematical Physics, volume I, Interscience, New York, 1953.
[17] Driscoll T. A. and Gottlieb H. P. W., Isospectral shapes with Neumann and alternating boundary conditions, Physical Rewiew E, 2003; 68:1–6.
[18] Fairweather G. and Johnson R. L., The method of fundamental solutions for problems in potential theory, In C.T.H. Baker and London J. F. Miler, Academic Press, editors, Treatment of integral equations by numerical methods, 1982.
[19] Fairweather G. and Karageorghis A., The method of fundamental solutions for elliptic boundary value problems, Adv Comput Math, 1998; 9:69-95.
[20] Fairweather G., Karageorghis A. and Martin. P. A., The method of fundamental solutions for scattering and radiation problems, Eng Anal Bound Elem, 2003; 27:759-769.
[21] Fox L., Henrici P. and Moler C. B., Approximations and bounds for eigenvalues of elliptic operators, SIAM J Numer Anal, 1967; 4:89-102.
[22] Golberg M. A. and Chen. C. S., The method of fundamental solutions for potential, Helmholtz and diffusion problems, In Boundary Integral Methods: Numerical and Mathematical Aspects, WIT Press, Computational Mechanics Publications, Boston, Southampton, 1999.
[23] Golberg M. A. and Chen C. S., Discrete Projection Methods for Integral Equations, Computational Mechanics Publications, Southampton, 1996.
[24] Hansen P. C., Rank-deficient and discrete ill-posed problems, SIAM, 1998.
[25] Johnson C., Numerical Solution of Partial Differential Equations by the Finite Element Method, Studentlitteratur, Lund, Sweden, 1987.
[26] Karageorghis A., Modified methods of fundamental solutions for harmonic and biharmonic problems with boundary singularities, Numer Meth for Partial Diff Eqns, 1992; 8:1-19.
[27] Karageorghis A., The Method of Fundamental Solutions for the calculation of the eigenvalues of the Helmholtz equation, Appl Math Letters, 2001; 14(7):837–842.
[28] Karageorghis A., Poullikkas A. and Berger J. R., Stress intensity factor computation using the method of fundamental solutions, Comput Mech, 2006; 37:445-454.
[29] Kitagawa T., Asymptotic stability of the fundamental solution method, J Comput Appl Math, 1991, 38:263–269.

[30] Kupradze V. D. and Aleksidze M. A., The method of fundamental equations for an approximate solution of certain boundary value problems, Comput Math Math Phys, 1964: 4:82–126.
[31] Lehmann R. S., Developments at an analytic corner of solutions of elliptic partial differential equations, J Math Mech, 1959; 8:729–760.
[32] Li Z. C., The Trefftz method for the Helmholtz equation with degeneracy, Appl Numer Math, 2008; 58:131–159.
[33] Marin L., Stable MFS solution to singular direct and inverse problems associated with the Laplace equation subjected to noisy data, CMES, 2008; 37:203-242.
[34] Mathon R. and Johnson R. L., The approximate solution of elliptic boundary-value problems by fundamental solutions, SIAM J Numer Anal, 1977; 14:638-650.
[35] Moler C. B. and Payne L. E., Bounds for eigenvalues and eigenfunctions of symmetric operators, SIAM J Numer Anal, 1968; 5:64–70.
[36] Poullikkas A., Karageorghis A. and Georgiou G., Methods of fundamental solutions for harmonic and bi-harmonic boundary value problems, Comput Mech, 1998; 21:416-423.
[37] Smyrlis Y. S. and Karageorghis A., Efficient implementation of the MFS: The three scenarios, J Comput Appl Math, 2009, 227:83-92.